Combined Atom Probe Tomography and TEM Investigations of CoCrFeNi, CoCrFeNi–Pd$_x$ ($x = 0.5$, 1.0, 1.5) and CoCrFeNi–Sn

J. Cornide[a], M. Calvo-Dahlborg[a,*], S. Chambreland[a], L. Asensio Dominguez[b],
Z. Leong[b], U. Dahlborg[a], A. Cunliffe[b], R. Goodall[b] and I. Todd[b]

[a]GPM-UMR6634-CNRS, University of Rouen, BP12, 76801 Saint-Etienne-du-Rouvray, France

[b]Department of Materials Science and Engineering, The University of Sheffield, Mappin Street, Sheffield S1 3JD, UK

The structure of a family of high entropy alloys based on the composition CoCrFeNi, to which Pd and Sn have been added, is presented. The results stem from combined investigations by atom probe tomography as well as by scanning and transmission electron microscopy on samples produced by arc melting. Although CoCrFeNi is of fcc structure, the sample is not homogeneous on atomic scale. The addition of Pd as a fifth element retains the fcc lattice with the indication of the coexistence of at least two additional phases. The addition of Sn changes the general structure considerably.

1. Introduction

The name high entropy alloys (HEA) has appeared about ten years ago to describe mostly single-phase alloys, often with fcc and/or bcc lattices, consisting of at least four metal components. Since then, a lot of studies have been published showing the exciting challenge to understand their formation by different production processes and to conceive alloys with suitable properties [1–6]. According to literature, HEAs have close to equimolar composition, form mostly fcc and/or bcc phases and solid solutions, i.e. the elements take random occupations on available lattice sites. However, additional intermetallic phases can also be found. Several publications have been devoted to finding rules for whether a melt after solidification forms a HEA or not. The understanding of the structure and the stability of HEAs is nevertheless still very incomplete and the mechanism behind the composition-property relationship is largely unclear.

In the present work, we focus on a basic HEA alloy (CoCrFeNi at equiatomic composition) to which is added a fifth element, Pd and Sn, in different amounts. The microstructure is examined by standard techniques: optical as well as scanning (SEM) and transmission (TEM) electron microscopy. The composition is measured by energy dispersive X-ray spectroscopy (EDS) and atom probe tomography (APT). Few APT studies on HEA have been reported until now and in only a few of them structural inhomogeneities could be observed [7–10]. In the present study, APT investigations were performed on alloys in which neutron (ND) and X-ray (XRD) diffraction measurements have suggested deviations from a single-phase

structure [11] and because fluctuations in composition were observed by EDS. For short, CCFN will be used in the following to denote the CoCrFeNi equimolar alloy.

2. Sample preparation and experimental techniques

The CCFN, CCFN–Pd$_x$ ($x = 0.5$, 1.0, 1.5) and CCFN–Sn alloys were prepared as presented elsewhere [2] from 99.9wt.% pure raw materials. Cylindrical rods were prepared by copper-mould suction casting into a water-cooled Cu hearth. Each alloy was remelted at least 4 times to ensure good mixing of the elements.

The observation of the morphology and the study of the composition of the different phases have been performed by SEM with a Zeiss 1530-XB microscope equipped with energy-dispersive X-ray detector. For revealing the microstructure, the standard metallographic procedure has been performed, i.e. grinding, polishing and etching using aqua regia solution. CCFN and CCFN–Pd samples were characterized by TEM in a JEOL 2010 microscope at 200 kV.

The study of the element distribution on the atomic scale has been performed by APT (energy compensated wide angle tomographic atom probe (ECOWATAP)) in 10^{-8} Pa ultrahigh vacuum, at 80 K, with 20% pulse fraction and 30 kHz pulse generation frequency on needle-shape samples prepared in a two steps electropolishing procedure by two solutions: 90% acetic acid + 10% perchloric acid and 98% butyl cellosolve + 2% hydrochloric acid. The GPM 3D software (Rouen/Cameca) was used for data reconstruction.

3. Results

The CCFN alloy observed by SEM exhibits a single phase microstructure formed by large columnar grains

*corresponding author; e-mail:
monique.calvo-dahlborg@uni-rouen.fr

(Fig. 1) up to 100 μm in width. SEM-EDX analysis reveals a homogeneous composition through the sample close to the nominal equimolar composition (Table I). No macroscopic segregation was observed. The locations in the ingot from where the TEM and APT samples were taken are shown in Fig. 2. The compositional differences

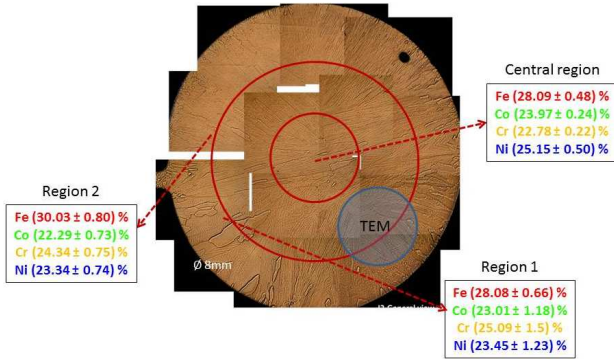Fig. 1. SEM image of CCFN alloy showing columnar grains.

Fig. 2. Light optical microscopy pictures of CCFN ingot. Arrows indicate APT and TEM sampling regions.
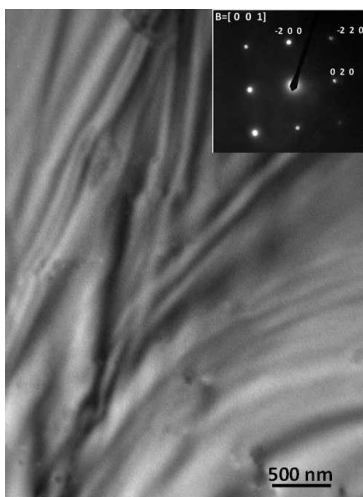

Fig. 3. Bright-field image of the CCFN alloy and the corresponding diffraction pattern along [0 0 1] zone axis.

observed between region 2 in Fig. 2 and the central region as well as region 1 can be explained as follows: region 2 is calculated from a single APT experiment, while the data obtained from central region and from region 1 are averages obtained from 2 and 4 experiments, respectively. Furthermore, due to the large grain size only one grain is measured in one single APT experiment. The representative bright-field TEM image in Fig. 3 shows a columnar grain. The corresponding diffraction pattern along the [0 0 1] zone axis in the inset indicates an fcc structure. The lattice parameter obtained from different patterns is $a_{\text{fcc}} = 3.56 \pm 0.03$ Å as calculated from different reflections. The standard deviation is smaller than the observational error, ± 0.05 Å.

TABLE I

Nominal composition and average compositions obtained by SEM-EDS from different regions in the CCFN ingot.

Element	Composition by SEM-EDS [at.%]	Nominal composition [at%]
Co	24.8 ± 0.4	25.0
Cr	25.8 ± 0.9	25.0
Fe	24.5 ± 0.6	25.0
Ni	24.9 ± 0.2	25.0

In order to determine the compositional differences in the ingot, several APT samples obtained from different regions in the ingot (Fig. 2) were investigated. Although some fluctuation in the lattice parameter [11] could be observed through the ingot, no macroscopic inhomogeneity could be detected. In order to investigate the chemical homogeneity at atomic scale, several boxes of $10 \times 10 \times 10$ nm^3 along the reconstructed volumes were used, each of them containing between 40000 and 50000 atoms (Fig. 4). Fluctuations (slightly above the error bar of 1 at.%, especially for Cr and Ni) but no defined clusters were observed in all the performed APT measurements.

CCFN–Pd$_x$ alloys of different compositions were investigated in order to study the influence of Pd as fifth component. A full characterization procedure has been performed including SEM-EDS on all compositions as well as APT and TEM-EDS for $x = 1.0$. An overall fcc structure is conserved for the three compositions as observed by TEM and confirmed by XRD [11]. The SEM observation reveals dendritic solidification as shown in Fig. 5. Table II presents the different compositions measured in both dendritic and interdendritic regions for all three investigated alloys. All alloys present a higher amount of Pd in the interdendritic region but in the case of CCFN–Pd$_{1.5}$ this difference is only about 2%. In addition, depletion in both Pd and Co as compared to nominal composition is observed for all compositions.

The APT reconstruction of CCFN–Pd$_{1.0}$ tip shows a homogeneous element distribution (Fig. 6). The arrow indicates the direction of the analysis. Enrichment of Pd is observed at the end of the tip. This can indicate that
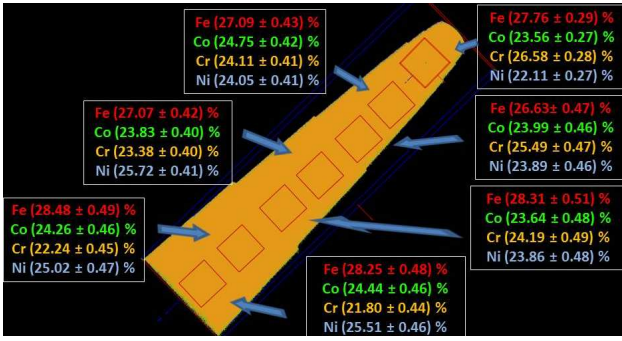
Fig. 4. 3D-reconstruction of a CCFN sample tip. Average atomic compositions in boxes of $10 \times 10 \times 10$ nm^3 are shown.

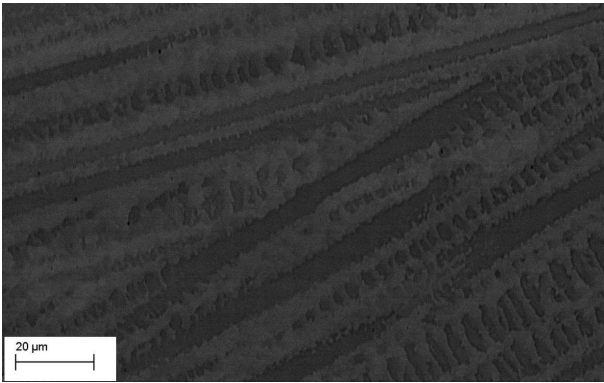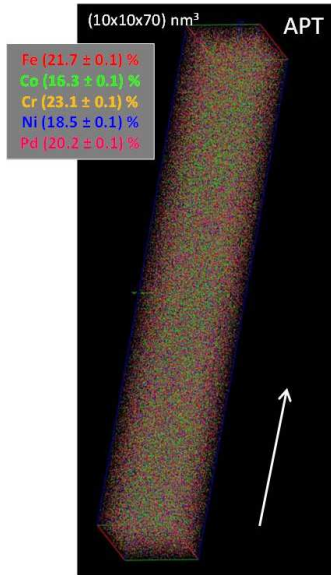Fig. 5. SEM image of the CCFN–Pd$_{1.0}$ alloy using BSE detector.

Fig. 6. APT reconstruction of a $10 \times 10 \times 70$ nm^3 CCFN–Pd$_{1.0}$ sample tip (4 million collected atoms). Dots represent the positions of individual atoms. The color correspondence is given in the legend indicating the average composition and the relative error. The arrow indicates the direction of the analysis.

Nominal composition and average compositions obtained by SEM-EDS of dendritic and interdendritic regions in the CCFN–Pd$_x$ sample for $x = 0.5$, 1.0 and 1.5.

x	Element	Dendritic	Interdendritic	Nominal
	Co	23.2 ± 0.4	20.4 ± 1.0	22.22
	Cr	22.2 ± 0.2	22.4 ± 0.2	22.22
0.5	Fe	23.4 ± 0.2	22.7 ± 0.2	22.22
	Ni	22.6 ± 0.3	22.4 ± 0.5	22.22
	Pd	8.5 ± 0.8	12.1 ± 0.8	11.11
	Co	18.1 ± 0.6	17.9 ± 0.3	20
	Cr	20.9 ± 1.1	20.4 ± 1.3	20
1.0	Fe	21.1 ± 1.7	19.4 ± 0.1	20
	Ni	22.5 ± 0.7	20.4 ± 1.1	20
	Pd	17.4 ± 0.4	21.9 ± 0.1	20
	Co	18.8 ± 0.2	18.1 ± 0.6	18.18
	Cr	18.4 ± 0.1	18.4 ± 0.2	18.18
1.5	Fe	19.4 ± 0.4	18.8 ± 0.3	18.18
	Ni	17.7 ± 0.3	17.6 ± 0.3	18.18
	Pd	25.6 ± 0.4	27.1 ± 1.2	27.27

the end of the tip is located in the interdendritic region, the Pd content being lower in the dendritic regions as compared to the interdendritic ones during the solidification process. The nearest neighbour analyses performed for the 1st, the 5th, and the 10th nearest neighbour do not show aggregation nor cluster. The composition of different $10 \times 10 \times 10$ nm^3 boxes along the tip axis is presented in Fig. 7. Depletion in Co is also observed.

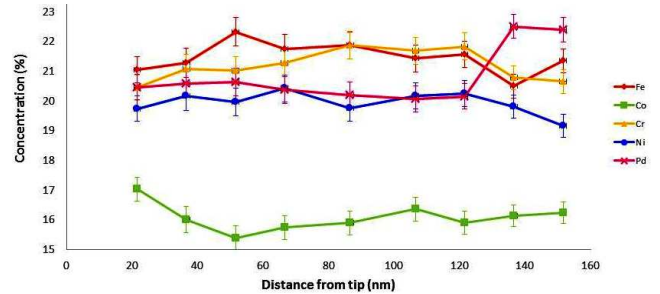Fig. 7. Composition measurement on CCFN–Pd$_{1.0}$ alloy on different statistical boxes in a reconstructed volume.

Nominal composition and average compositions obtained by SEM-EDS of dendritic and interdendritic regions in the CCFN–Sn$_{1.0}$ sample.

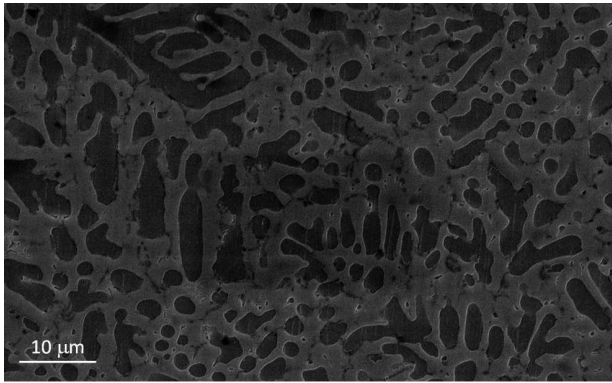| Element	Dendrites	Interdendrites	Nominal
Cr	26.2 ± 1.9	15.7 ± 3.0	20
Fe	26.7 ± 2.2	15.6 ± 2.8	20
Co	24.7 ± 1.7	17.1 ± 1.7	20
Ni	13.6 ± 1.8	23.8 ± 2.5	20
Sn	8.8 ± 4.0	27.8 ± 5.0	20

Fig. 8. SEM image of the CCFN–Sn$_{1.0}$ alloy showing dendrites.

The general observation of CCFN–Sn$_{1.0}$ alloy shows a dendritic solidification (Fig. 8) process in the sample. By SEM-EDS observation the element composition presents a homogeneous distribution along the ingot. The study of the different features shows that the dendrites are depleted in Sn and Ni and enriched in Fe–Co–Cr while interdendritic regions show the opposite behaviour (Table III). XRD investigations have confirmed the existence of several phases [11].

4. Discussion

The CCFN alloy, containing two fcc phases from ND and XRD results [11], does not seem to be homogeneous on atomic scale. APT analysis on a nanometer scale, and also EDS on a higher scale, reveals a fluctuation of composition not only through the ingot as indicated by XRD. This observation is similar to the discrepancies reported in [12, 13]. This fluctuation of composition may be understood by the excess of entropy existing in these materials which thus results in a neither random nor periodic occupation of the fcc sites by the different atoms all having very similar atomic radii.

When another element such as Pd is added to CCFN, the structure retains its overall fcc character for the three studied compositions. Although dendrites can be clearly observed, the difference in composition between the dendritic and the interdendritic domains is small. The observed depletion in both Co and Pd suggests the existence of another phase.

When Sn is added, clear dendritic microstructure is observed in the alloy of equimolar composition as seen in Fig. 8. XRD reveals two phases, an orthorhombic one and an fcc one [11]. Table III indicates a clear difference between the two phases: one dendritic richer in Fe, Co and Cr, one interdendritic richer in Ni and Sn.

5. Conclusions

The basic CoCrFeNi high entropy alloy is not homogeneous on atomic scale.

The different elements although of similar atomic size, are distributed neither randomly nor periodically in the alloy.

With the addition of Pd as fifth element to the alloy, the overall fcc structure remains although there is strong indication for the existence of at least two additional phases.

The addition of Sn leads to the separation of the alloy into two phases with different composition and crystalline structure.

Acknowledgments

References

[1] Y. Zhang, T.T. Zuo, Z. Tang, M.C. Gao, K.A. Dahmen, P.K. Liaw, Z.P. Lu, *Prog. Mater. Sci.* **61**, 1 (2014).

[2] A. Cunliffe, J. Plummer, I. Figueroa, I. Todd, *Intermetallics* **2**, 204 (2012).

[3] R. Raghavan, K.C. Hari Kumar, B.S. Murty, *J. Alloys Comp.* **54**, 152 (2012).

[4] K.G. Pradeep, N. Wanderka, P. Choi, J. Banhart, B.S. Murty, D. Raabe, *Acta Mater.* **61**, 4696 (2013).

[5] Z. Wu, H. Bei, F. Otto, G.M. Pharr, E.P. George, *Intermetallics* **46**, 131 (2014).

[6] M.H. Tsai, J.W. Yeh, *Mater. Res. Lett.* **2**, 107 (2014).

[7] S. Singh, N. Wanderka, K. Kiefer, K. Siemensmeyer, J. Banhart, *Ultramicroscopy* **111**, 619 (2011).

[8] S. Singh, N. Wanderka, B.S. Murty, U. Glatzel, J. Banhart, *Acta Mater.* **59**, 182 (2011).

[9] A. Manzoni, H. Daoud, S. Mondal, S. van Smaalen, R. Völkl, U. Glatzel, N. Wanderka, *J. Alloys Comp.* **552**, 430 (2013).

[10] M.J. Yao, K.G. Pradeep, C.C. Tasan, D. Raabe, *Scr. Mater.* **72–73**, 5 (2014).

[11] U. Dahlborg, J. Cornide, M. Calvo-Dahlborg, T.C. Hansen, Z. Leong, L. Asensio Dominguez, S. Chambreland, A. Cunliffe, R. Goodall, I. Todd, *Acta Phys. Pol. A* **128**, 552 (2015).

[12] Y.F. Kao, T.J. Chen, S.K. Chen, J.W. Yeh, *J. Alloys Comp.* **488**, 57 (2009).

[13] W.R. Wang, W.L. Wang, S.C. Wang, Y.C. Tsai, C. Lai, J.W. Yeh, *Intermetallics* **26**, 44 (2012).